ACS Energy LETTERS

http://pubs.acs.org/journal/aelccp

Graphite-Based Lithium-Free 3D Hybrid Anodes for High Energy Density All-Solid-State Batteries

Xing Xing, Yejing Li, Shen Wang, Haodong Liu, Zhaohui Wu, Sicen Yu, John Holoubek, Hongyao Zhou, and Ping Liu*

Cite This: *ACS Energy Lett.* 2021, 6, 1831−1838

Read Online

ACCESS | Metrics & More | Article Recommendations | Supporting Information

ABSTRACT: **All-solid-state lithium batteries often suffer from dendrite-driven shorting. Here, a lithium-free 3D anode design is reported to help address this challenge. Upon controlling the graphite anode and lithium metal oxide cathode capacity ratio, lithium metal deposition is intentionally induced in the pores formed by the 3D framework of the graphite and lithium thiophosphate-based solid electrolyte. By facilitating lithium deposition away from the interface between the anode composite and the solid-state electrolyte layer, this designed electrode can significantly mitigate the short-circuit problem in the battery. The 3D anode design demonstrates a 3-fold increase in critical current density over a planar lithium metal electrode when evaluated in a symmetric cell. Moreover, the lithium-free all-solid-state battery with a 3D anode and a Li-$Ni_{0.85}Co_{0.10}Al_{0.05}O_2$ (NCA) cathode also exhibits highly improved cycle life and Coulombic efficiency compared to the baseline cells. This electrode design provides a promising approach toward a high energy density, long life, and low-cost technology.**

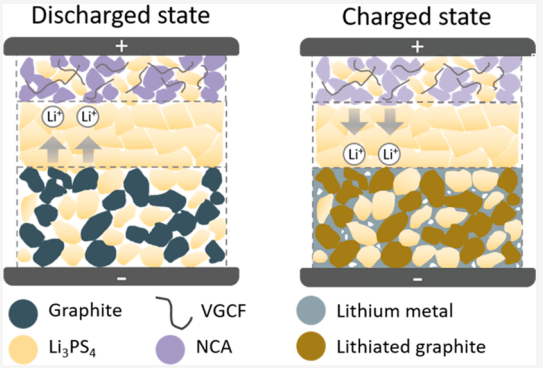

All-solid-state batteries (ASSBs) have emerged as promising next-generation batteries because of their potential to provide high energy density and enhanced safety.[1−9] Utilization of Li metal as the anode in ASSBs is the ideal choice. However, challenges remain with regard to the stability of the Li metal anode, such as dendrite formation and large volume changes during cycling, which result in mechanical degradation at the interface between the anode and solid-state electrolyte (SSE).[10−16] This degradation not only contributes to a significant reduction of cell life but also leads to potential cell internal short circuits.[17−21] Strategies have been developed to analyze and resolve the interface issues caused by Li metal anode, such as adding a self-healing component into the SSE, softening the SSE with polymers, engineering of interlayers, and rational control of Li metal deposition based on theoretical studies.[10,11,16,22−37]

One particularly promising approach is to apply a 3D anode network, which hosts the deposited lithium metal. Such hosts serve to mitigate dendrite growth toward the SSE, minimize volume change during cycling, and maintain the integrity of the anode/electrolyte interface.[6,8,14,34,36,38−42] However, unlike liquid cells where electrolytes can flow into the 3D network and conduct ions, it is difficult to extend these anode networks into ASSBs while maintaining ionically conducting pathways.[34,43] An early example is the use of a porous garnet SSE as a 3D ionic framework for Li metal deposition.[14,40] The large contact area between Li metal and this garnet SSE reduced the local current density at the interface, producing a small overpotential and homogeneous Li metal deposition. The electronic pathway relies on lithium metal itself because the SSE network has no electronic conductivity. Various types of nickel foam and carbon matrices have also been examined as Li metal anode hosts, which improved the interfacial stability by maintaining anode structure during cycling.[4,10,15,16,22,23,28] However, these hosts, while electronically conducting, have been limited because of negligible ionic conductivities. As a result, Li metal plating and stripping, which require ion transport, need to be initiated at the electrolyte/3D-host interface where the formation of dendrites is still detrimental.[10−12,40,44] It follows that an ideal host design should be a

Received: March 25, 2021
Accepted: April 15, 2021

https://doi.org/10.1021/acsenergylett.1c00627
ACS Energy Lett. 2021, 6, 1831−1838

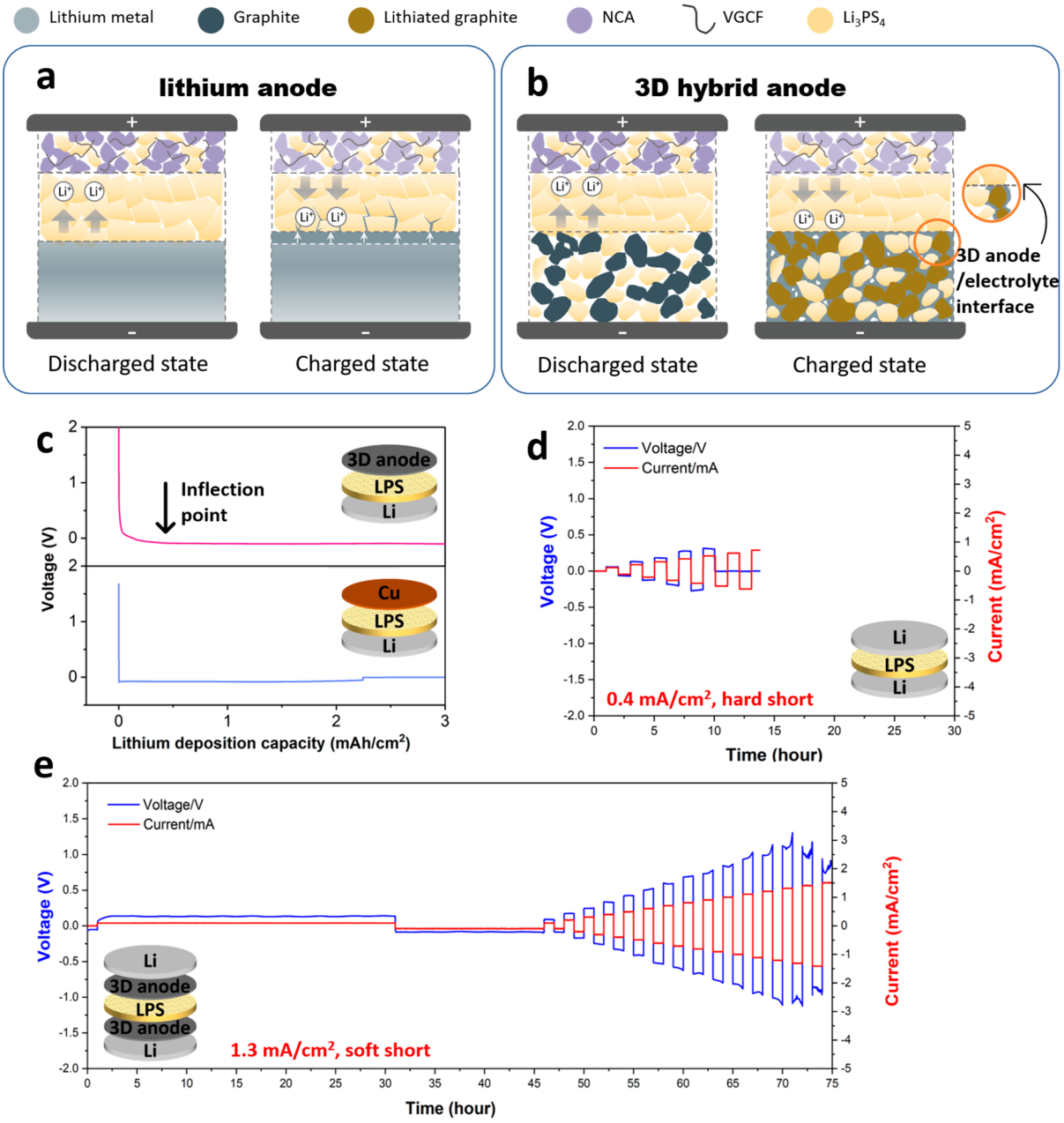

Figure 1. Lithium metal plating and stripping in all-solid-state lithium metal batteries. (a) Schematic of an all-solid-state battery with lithium metal as anode. (b) Schematic of an all-solid-state battery with hybrid 3D anode. Unlike the planar lithium metal, the 3D anode design encourages lithium deposition in the porous host and away from the electrolyte interface. (c) Voltage profiles of Li deposition in Li-3D anode cell and Li−Cu cell. (d) Critical current density test of a Li/LPS/Li cell. (e) Critical current density test of a Li/3D/LPS/3D/Li symmetric cell.

mixed ionic and electronic conducting 3D anode network that is lithiophilic and is mechanically processable at room temperature. This design will effectively shift Li deposition away from the interface, thus extending the cell cycle life.[31]

Graphite, which is cheap and abundant, has demonstrated long cyclability with little volume change in all-solid-state Li-ion batteries.[25,29,44−46] After lithiation, the product LiC_6 is thermodynamically stable with Li metal and has both electronic and ionic conductivity. Moreover, LiC_6 is shown to be lithiophilic and can facilitate Li metal deposition.[44,47,48] These properties suggest graphite can fit the aforementioned design requirements as a material for 3D anode networks in ASSBs. In the meantime, lithium thiophosphate (LPS) has a high ionic conductivity (2.01×10^{-3} S cm^{-1} at room temperature) and low Young's (~20 GPa) and shear (~7 GPa) elastic moduli. These properties allow LPS to be densified at low temperature by mechanical compression, a distinct advantage over oxide-based electrolytes.[25,49,50] Therefore, an LPS/graphite composite is a good candidate to demonstrate the proof of concept of improving Li deposition, although the chemical stability between Li and LPS remains an active topic of research.[51−54]

Considering these principles, we report a 3D mixed conductive anode network composed of lithiated graphite and LPS SSE, which is low-cost and facile to fabricate. After uniformly distributing extra Li metal into the voids during cell

https://doi.org/10.1021/acsenergylett.1c00627
ACS Energy Lett. 2021, 6, 1831−1838

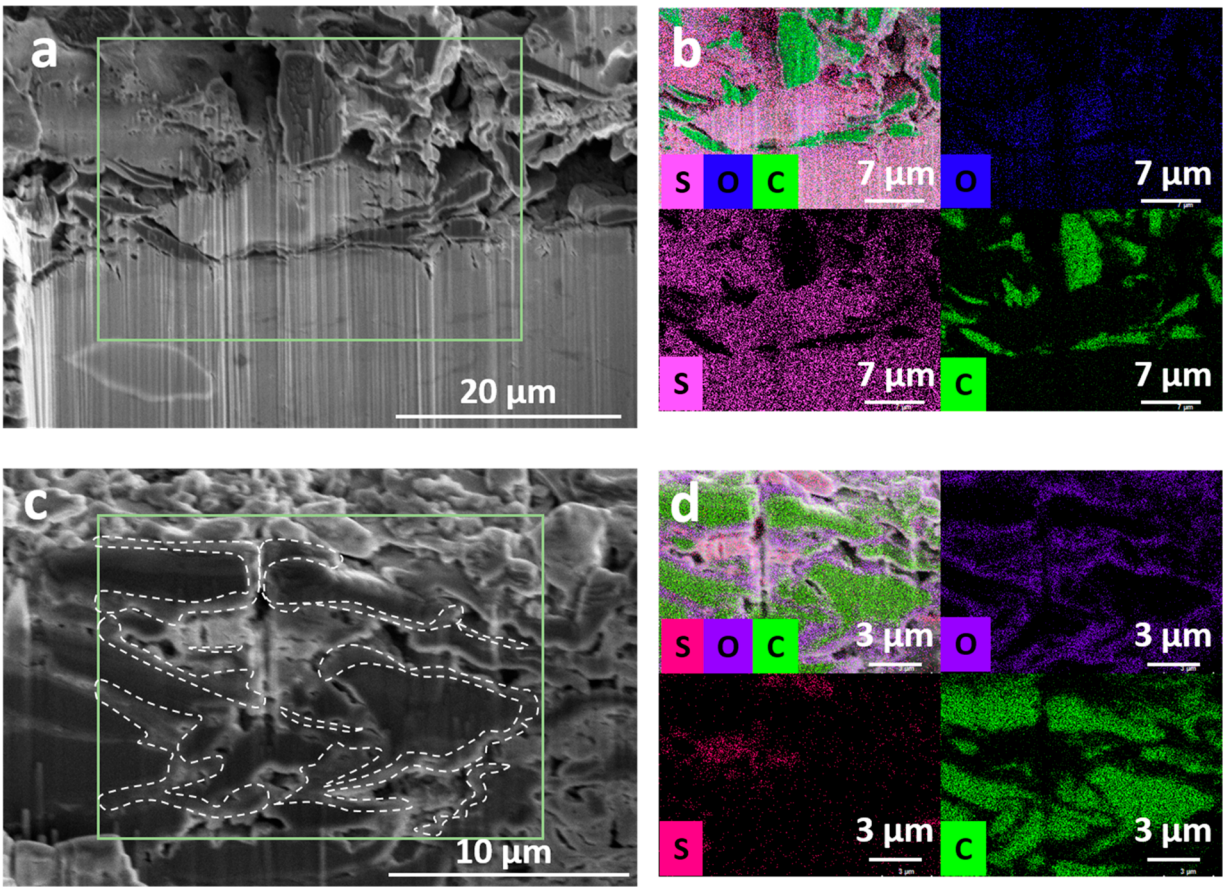

Figure 2. Lithium metal deposition distribution in 3D anode. (a) SEM image and (b) EDX mappings of cross section of Li-3D anode cell after lithiation to 0 V. (c) SEM image and (d) EDX mappings of cross-section of Li-3D anode cell after lithiation and an additional 1 mA cm^{-2} lithium deposition. The thin slices between the dashed white lines in panel c illustrate lithium metal deposition, which corresponds to intense oxygen signals but no carbon signals.

operation, a 3D graphite−lithium hybrid anode was realized. Moreover, we employed this 3D anode into a conventional solid-state battery by gradually reducing the amount of graphite anode to intentionally induce lithium metal deposition, thus achieving a "lithium-free" design. Such an approach enables an assessment of lithium cycling efficiency because of the limited amount of active lithium. In addition, this approach is compatible with a manufacturing process identical to that of solid-state lithium-ion batteries, enabling a gradual transition to solid-state lithium metal batteries.

The design of a solid-state battery with a 3D lithium−graphite hybrid anode is schematically shown in Figure 1. When Li metal foil is used as the anode, because of its volume change during cycling, the interface between the anode and the SSE layer shifts in the cell. Moreover, the uneven Li metal deposition results in dendrites which can penetrate into the SSE layer, causing the short circuits (Figure 1a). In contrast, a 3D mixed conducting anode network composed of graphite and LPS SSE is shown in Figure 1b. During charge, after fully lithiating the graphite, the lithium metal plates into the voids inside the 3D network, which is both electronically and ionically conducting. By shifting lithium metal deposition away from the interface between the anode composite and the SSE layer, the interface maintains its integrity. The high surface area of the graphite anode reduces effective current density and mitigates lithium dendrite formation.

We examined the advantage of the 3D graphite/LPS host in preventing cell short circuit in terms of lithium deposition capacity and cycling current. We have found that without LPS in the anode, graphite in itself does not have sufficient ion conductivity to facilitate 3D lithium deposition (see Discussion One and Figure S1 in the Supporting Information). Figure 1c compares the voltage profiles of the Li/LPS/3D anode cell and a baseline Li−Cu cell when lithium was continuously deposited until the cells experienced short circuit. The Li−Cu cell hard shorted after only ∼2.2 mAh cm^{-2} of lithium was deposited. In contrast, the 3D anode cell did not short after 3 mAh cm^{-2}. We estimated the porosity of the 3D anode to be ∼41% based on graphite mass (1.7 mg cm^{-2}) and electrode thickness (30 μm) observed by SEM in Figure S2a, and the complete filling of the pores corresponds to ∼3 mAh cm^{-2} capacity. This capacity is equivalent to around 900 mAh g^{-1} of anode composite, a practically relevant value because previous models have shown the effect of further raising the anode specific capacity on cell energy density is minimal.[16,55,56] A detailed calculation on maximum lithium storage capacity is provided in the Supporting Information (Discussion Two). The inflection point at ∼0.5 mAh cm^{-2} on the discharge voltage profile of the 3D anode cell implies the end of graphite lithiation and the start of lithium metal plating.

Critical current density, defined as the maximum current density when cell shorting occurs, was then measured to examine the effect of the 3D host. As shown in Figure 1d, for a

https://doi.org/10.1021/acsenergylett.1c00627
ACS Energy Lett. 2021, 6, 1831−1838

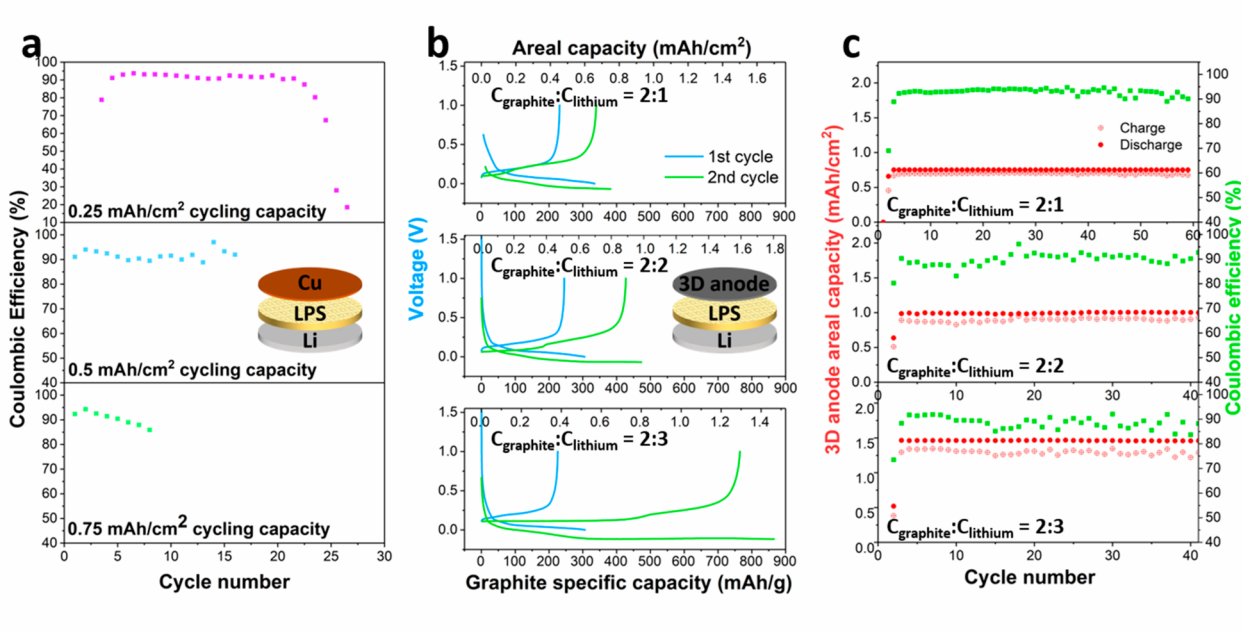

Figure 3. Electrochemical performance of the Li−Cu cells and Li-3D anode cells. (a) Coulombic efficiency of Li−Cu cell with 0.25, 0.5, and 0.75 mAh cm^{-2} lithium cycling capacity. (b) Voltage profiles and (c) cycling performance of Li-3D anode cell with 0.75, 1, and 1.25 mAh cm^{-2} cycling capacity.

Li/LPS/Li symmetric cell, the short circuit occurred at 0.4 mA cm^{-2}. Each step is 30 min, and the increment of current density at each step is 0.1 mA cm^{-2}, comparable to previously reported testing parameters.[57,58] To test the effectiveness of the 3D anode, a Li/3D/LPS/3D/Li cell was fabricated. As shown in Figure 1e, before the critical current density test, 3 mAh cm^{-2} lithium metal capacity was first stripped from the left lithium chip and deposited into the 3D graphite region on the right through LPS SSE, followed by 1.5 mAh cm^{-2} lithium metal capacity being stripped back to the left 3D graphite electrode to fabricate a symmetric 3D hybrid graphite/lithium anode cell. When subjected to ramped-rate cycling, the critical current density of the symmetric 3D anode cell was 1.4 mA cm^{-2}, where the cell showed signs of a soft short (Figure 1e). These results represent a significant improvement from previously reported data as summarized in Table S1 and provide further evidence of the benefit of the 3D anode to enhance battery stability.

Scanning electron microscopy (SEM) was then applied to examine the lithium deposition morphology. As shown in Figure S3, after 1 mAh cm^{-2} lithium metal deposition on planar Cu, a lithium metal film was clearly observed between the SSE and Cu. Moreover, spike-shaped lithium penetrating into the LPS SSE was observed. After the top LPS SSE layer is removed (Figure S3), the deposited lithium metal islands with various thickness are nonuniformly distributed on the surface of Cu, while some areas show a bare Cu surface. In comparison, we applied focused ion beam (FIB)-SEM to examine the lithium deposition in a 3D anode. First, the cross section of a fully lithiated graphite electrode without further lithium metal deposition is shown in Figure 2a. The relatively dark regions reflect a higher electronic conductivity, which are attributed to either lithiated graphite or lithium metal, and the relatively lighter regions represent the LPS solid electrolyte, consistent with the energy-dispersive X-ray spectroscopy (EDX) mappings as shown in Figure 2b. There is no lithium metal observed in this electrode. Figure 2c,d shows the results for the overlithiated 3D anode. The area with C signals in the EDX mapping is smaller than the dark region in the SEM images. The rest of the dark region corresponds to strong O signals, which is attributed to lithium metal. Consequently, we conclude that lithium metal is deposited as a thin layer on the surface of the lithiated graphite particles. Further evidence for the 3D distribution of lithium metal, including its presence near the current collector, is provided in the Supporting Information (Discussion Three and Figure S2).

To further understand the mechanism of lithiated graphite for facilitating 3D lithium metal deposition, we also investigated alternative materials as the anode host. As shown in Figure S4, an LTO-based 3D anode host was fabricated and tested with the same cell configuration. LTO was chosen because it is known to be stable at 0 V.[59] After overlithiation, lithium metal particles were observed at the 3D anode/electrolyte interface, but no lithium metal was found inside the 3D LTO host. A plausible explanation is that lithiated graphite is much more lithiophilic than LTO, a quality that is essential for the success of the 3D concept.

We next examine the 3D anode effects by comparing the cycle life and Coulombic efficiency (CE) of Li−Cu and Li-3D anode cells. As shown in Figure 3a, at a plating capacity of 0.25 mAh cm^{-2}, the Li−Cu cell lasted only 22 cycles with an average CE of ∼91%. This CE is comparable to previously reported values and reflects the side reactions between LPS SSE and Li metal.[26,50,57,58,60] At the 22nd cycle, there is a clear hard short during lithium deposition, as evident in the sudden drop of cell voltage to 0 V as shown in Figure S5a. Increasing lithium deposition capacity to 0.5 and 0.75 mAh cm^{-2} results in hard shorts in 16 cycles and 8 cycles, respectively. However, with the introduction of 3D anodes, the cell life was significantly extended in the same tests. As shown in the voltage profiles in Figure 3b, the graphite anodes were first fully lithiated and delithiated to confirm the graphite capacity.

https://doi.org/10.1021/acsenergylett.1c00627
ACS Energy Lett. 2021, 6, 1831−1838

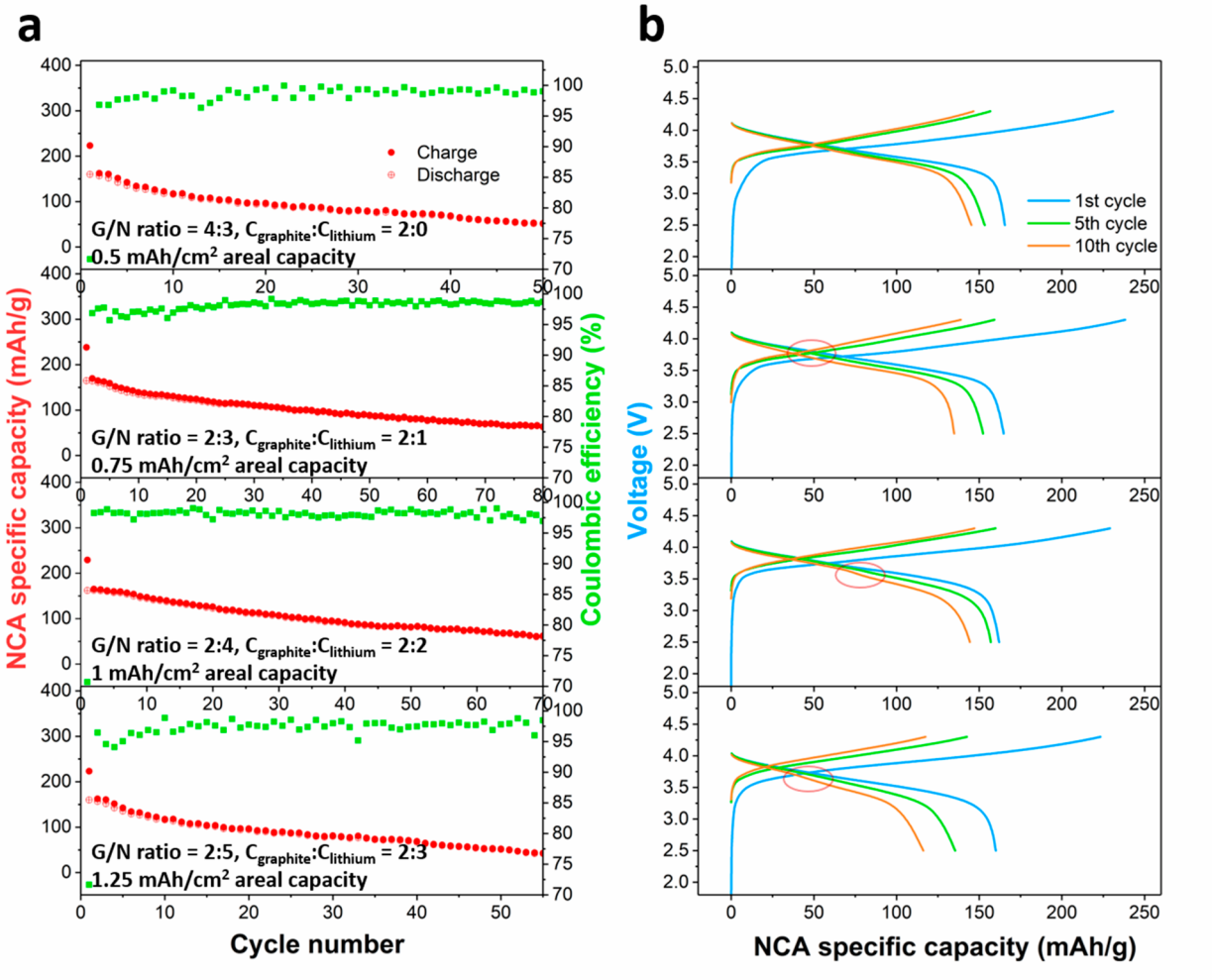

Figure 4. Electrochemical performance of NCA-3D anode cells. (a) Cycling performance and (b) voltage profiles of the NCA-3D anode cell with graphite/NCA cathode capacity (G/N) ratio of 4:3, 2:3, 2:4, and 2:5.

During the second cycle, the electrode is then lithiated with a capacity beyond the storage capacity of graphite in the form of lithium metal. To facilitate comparison with the reference Li−Cu cells, the lithium metal capacity was chosen to be 0.25, 0.5, and 0.75 mAh cm^{-2}. Because the graphite anode has a capacity of 0.5 mAh cm^{-2}, the capacity ratios, $C_{graphite}$:$C_{lithium}$, for the three electrodes are 2:1, 2:2, and 2:3, which also translate to the corresponding anode specific capacities normalized to the weight of graphite as 382, 479, and 864 mAh g^{-1}, respectively. The Li-3D cell with 0.75 mAh/cm^2 total cycling capacity in Figure 3b has 0.5 mAh cm^{-2} attributed to lithium storage in graphite while 0.25 mAh cm^{-2} is lithium metal. As shown in Figure 3c, this cell cycled for more than 60 cycles without shorting, in contrast to the 22 cycles for the Li−Cu cell with the same 0.25 mAh cm^{-2} lithium metal capacity. Moreover, the average CE also increased to >94%. Likewise, 3D anodes with lithium metal capacities of 0.5 and 0.75 mAh cm^{-2} were cycled for more than 40 cycles without shorting, a vast improvement over their Li−Cu baseline counterparts. Although post-mortem analysis shows that the stability between LPS and Li needs further improvement (see Discussion Four and Figures S6 and S7 in the Supporting Information), the highly improved cycling performance clearly demonstrates the positive effects of hybrid anode on electrochemical cycling stability.

The 3D anode was then employed to construct all-solid-state full cells with a $LiNbO_3$-coated $LiNi_{0.85}Co_{0.10}Al_{0.05}O_2$ (NCA) cathode.[61−63] Previous reports have shown that the $LiNbO_3$ coating can greatly improve the compatibility between NCA and the LPS electrolyte. As shown in the SEM and EDX analysis of coated NCA material in Figure S9, the uniform distribution of Nb indicates the complete coating of $LiNbO_3$. The capacity and cycling stability of NCA is comparable to previously reported values (Figure S10).[22,27,64−66]

The performance of "lithium-free" NCA-Cu cells with different areal capacities is shown in Figure S11. Figure S11a shows the capacity retention and voltage profile evolution of a cell with a capacity of 0.25 mAh cm^{-2}. Because of the irreversible capacity of NCA during the first cycle, there was excess lithium stored at the anode at the end of cell discharge. Consequently, the cell operates as the one with excess active lithium when cell degradation is mainly due to gradual cathode capacity loss. After about 6 cycles, the degradation of the CE and cycling capacity accelerated, implying the excess lithium was consumed because of the instability of deposited Li metal with the electrolyte. Starting with the seventh cycle, the cell capacity retention reflects the consumption of active lithium. The cell ran out of lithium in ∼40 cycles, with a calculated efficiency of 94.8% per cycle. Similar performance trends were

https://doi.org/10.1021/acsenergylett.1c00627
ACS Energy Lett. 2021, 6, 1831−1838

observed for NCA cathodes with capacities of 0.5 and 0.75 mAh cm^{-2} as shown in Figures S11b and S10c. Both cells suffered more rapid capacity loss with efficiencies of 94.7% and 92.2%, respectively. The poor cycling performance indicates that the consumption of active lithium at the anode/electrolyte is substantial.

In contrast, the 3D-NCA cells delivered much improved performance (Figure 4). At a graphite/NCA cathode capacity (G/N) ratio of 4/3, the graphite-NCA full cell is a lithium-ion battery involving no lithium metal deposition and shows a comparable cycling stability to the Li-NCA cell, indicating that the graphite/LPS interface is quite stable. The excess lithium provided by the NCA cathode during the first charging process was apparently sufficient to compensate for any parasitic loss on the anode. Such stability is likely attributed to the limited volume change of the graphite anode. As the G/N ratio decreases below 1, lithium metal starts to deposit on the surface of graphite, resulting in a hybrid anode battery. As shown in Table S2, the cell energy density increases about two times as the G/N ratio decreases from 2 to 0.4, implying the significant improvement in energy density by depositing lithium metal into the 3D host. At a G/N ratio of 2:3, 0.5 mAh cm^{-2} capacity was expected to be stored in graphite and 0.25 mAh cm^{-2} was as lithium metal, which corresponds to ~390 mAh g^{-1} effective graphite specific capacity. This capacity ratio can be confirmed by analyzing the cell discharge profile. When anode metallic lithium is exhausted and lithium is deintercalated from the graphite, the anode potential will increase, which results in an inflection point on the discharge profile, as the marked region in the voltage profiles. (Thus, the average voltage of a 3D-NCA cell is slightly lower than a Li-NCA cell.) This 3D-NCA cell retained 38% of its capacity after more than 80 cycles with a 98.8% average CE. This performance is a vast improvement over the case of Cu-NCA shown in Figure S4a, which lost all its capacity within 40 cycles. Increasing the total areal capacity to 1 mAh cm^{-2} corresponds to a G/N ratio of 2:4 and ~520 mAh g^{-1} graphite specific capacity. The cell capacity retention is 36% after 70 cycles with a 98.5% average CE. Further increasing the areal capacity to 1.25 mAh cm^{-2} increases the G/N ratio to 2/5 and the effective graphite specific capacity to ~650 mAh g^{-1}. This cell retained 27% of its capacity after 55 cycles with a 97.5% average CE.

The employment of a 3D anode thus greatly improved both cell life and CE. It is worth noting that the observed higher CE values are not simply due to the reduced lithium metal amount in a hybrid 3D anode. We calculated the respective CE for the graphite portion and lithium metal portion in the 3D anode for the 3D-NCA cell shown in Figure 4 (see Discussion Five in the Supporting Information). A CE value of 97.87% for lithium metal was obtained, a significant improvement over the value of 94.8% observed for a planar Li metal electrode (Figure S11). This improvement in efficiency, despite the large contact area between Li and LPS in the 3D structure and chemical compatibility issues, demonstrates the benefit of the 3D design, i.e., the reduced effective current density and lack of dendrite formation. As shown by the EIS analysis in Figure S12, improvements in the compatibility between Li and LPS are still needed to realize longer cycle life. Overall, the 3D anode shows much improved cycle life with high CE in a "lithium-free" cell configuration in comparison to a planar copper electrode.

In summary, we have shown that overlithiated graphite can serve as a convenient 3D host for lithium metal plating in a solid-state battery, thus moving most of the deposited lithium away from the interface between anode and SSE. This design significantly improves the critical current density and cycle life in half cells. Moreover, this design enables the fabrication of "lithium-free" solid-state 3D-NCA cells. Upon simply adjusting the graphite-to-NCA mass ratio, lithium metal is plated in the porous framework formed by the 3D lithiated graphite and LPS electrolyte. These cells show much improved cycle life and CE as compared to the copper-based baseline cells. This work clearly illustrates the benefits of depositing Li metal in a 3D mixed conductive network. With further improvement in electrolyte stability and microstructure design, the 3D anode approach provides a convenient, promising pathway toward high energy density, long life, and low-cost all-solid-state batteries.

■ ASSOCIATED CONTENT

Supporting Information

The Supporting Information is available free of charge at https://pubs.acs.org/doi/10.1021/acsenergylett.1c00627.

Experimental section, discussion on pure graphite anode, discussion on lithium deposition distribution in 3D anode, critical current tests summary, lithium metal deposition morphology in Li−Cu cell and Li-LTO cell, voltage profiles of Li−Cu cells, post-mortem analysis of Li-3D cell, electrochemical behavior of NCA-Li cells and NCA-Cu cells, energy density projection (PDF)

■ AUTHOR INFORMATION

Corresponding Author

Ping Liu − *Department of Nanoengineering, University of California, San Diego, La Jolla, California 92093, United States*; orcid.org/0000-0002-1488-1668; Email: piliu@eng.ucsd.edu

Authors

Xing Xing − *Department of Nanoengineering, University of California, San Diego, La Jolla, California 92093, United States*

Yejing Li − *Department of Nanoengineering, University of California, San Diego, La Jolla, California 92093, United States*

Shen Wang − *Department of Nanoengineering, University of California, San Diego, La Jolla, California 92093, United States*

Haodong Liu − *Department of Nanoengineering, University of California, San Diego, La Jolla, California 92093, United States*

Zhaohui Wu − *Department of Nanoengineering, University of California, San Diego, La Jolla, California 92093, United States*

Sicen Yu − *Department of Nanoengineering, University of California, San Diego, La Jolla, California 92093, United States*

John Holoubek − *Department of Nanoengineering, University of California, San Diego, La Jolla, California 92093, United States*; orcid.org/0000-0003-0015-4512

Hongyao Zhou − *Department of Nanoengineering, University of California, San Diego, La Jolla, California 92093, United States*

Complete contact information is available at: https://pubs.acs.org/10.1021/acsenergylett.1c00627

Notes

The authors declare no competing financial interest.

■ ACKNOWLEDGMENTS

This work has been supported by the Advanced Research Projects Agency-Energy, U.S. Department of Energy, under Contract No. DE-AR0000781. Part of this work was performed at the San Diego Nanotechnology infrastructure (SDNI) of the UCSD, a member of the National Nanotechnology Coordinated infrastructure, supported by the National Science Foundation (Grant ECCS-1542148).

■ REFERENCES

(1) Liu, H.; Yue, X.; Xing, X.; Yan, Q.; Huang, J.; Petrova, V.; Zhou, H.; Liu, P. A Scalable 3D Lithium Metal Anode. *Energy Storage Mater.* **2019**, *16*, 505−511.

(2) Wu, Z.; Xie, Z.; Yoshida, A.; Wang, Z.; Hao, X.; Abudula, A.; Guan, G. Utmost Limits of Various Solid Electrolytes in All-Solid-State Lithium Batteries: A Critical Review. *Renewable Sustainable Energy Rev.* **2019**, *109*, 367−385.

(3) Liu, H.; Wang, X.; Zhou, H.; Yan, Q.; Lim, H.-D.; Xing, X.; Meng, Y. S.; Liu, P. Structure and Solution Dynamics of Lithium Methyl Carbonate as a Protective Layer For Lithium Metal. *ACS Appl. Energy Mater.* **2018**, *1* (5), 1864−1869.

(4) Nam, Y. J.; Oh, D. Y.; Jung, S. H.; Jung, Y. S. Toward Practical All-Solid-State Lithium-Ion Batteries with High Energy Density and Safety: Comparative Study for Electrodes Fabricated by Dry- and Slurry-Mixing Processes. *J. Power Sources* **2018**, *375*, 93−101.

(5) Wang, J.; He, Y. S.; Yang, J. Sulfur-Based Composite Cathode Materials for High-Energy Rechargeable Lithium Batteries. *Adv. Mater.* **2015**, *27* (3), 569−575.

(6) Cheng, X. B.; Zhang, R.; Zhao, C. Z.; Wei, F.; Zhang, J. G.; Zhang, Q. A Review of Solid Electrolyte Interphases on Lithium Metal Anode. *Adv. Sci.* **2016**, *3* (3), 1500213.

(7) Li, X.; Liang, J.; Zhang, K.; Hou, Z.; Zhang, W.; Zhu, Y.; Qian, Y. Amorphous S-rich $S_{1-x}Se_x$/C ($x \leq 0.1$) composites promise better lithium−sulfur batteries in a carbonate-based electrolyte. *Energy Environ. Sci.* **2015**, *8* (11), 3181−3186.

(8) Lee, J. T.; Zhao, Y.; Kim, H.; Cho, W. Il; Yushin, G. Sulfur Infiltrated Activated Carbon Cathodes for Lithium Sulfur Cells: The Combined Effects of Pore Size Distribution and Electrolyte Molarity. *J. Power Sources* **2014**, *248*, 752−761.

(9) Patel, M. U. M.; Gaberscek, M.; Dominko, R.; Demir-Cakan, R.; Morcrette, M.; Tarascon, J.-M. Li-S Battery Analyzed by UV/Vis in Operando Mode. *ChemSusChem* **2013**, *6* (7), 1177−1181.

(10) Gao, Z.; Sun, H.; Fu, L.; Ye, F.; Zhang, Y.; Luo, W.; Huang, Y. Promises, Challenges, and Recent Progress of Inorganic Solid-State Electrolytes for All-Solid-State Lithium Batteries. *Adv. Mater.* **2018**, *30* (17), 1705702.

(11) Yang, C.; Zhang, L.; Liu, B.; Xu, S.; Hamann, T.; McOwen, D.; Dai, J.; Luo, W.; Gong, Y.; Wachsman, E. D.; Hu, L. Continuous Plating/Stripping Behavior of Solid-State Lithium Metal Anode in a 3D Ion-Conductive Framework. *Proc. Natl. Acad. Sci. U. S. A.* **2018**, *115* (15), 3770−3775.

(12) Li, Y. Q.; Li, J. C.; Lang, X. Y.; Wen, Z.; Zheng, W. T.; Jiang, Q. Lithium Ion Breathable Electrodes with 3D Hierarchical Architecture for Ultrastable and High-Capacity Lithium Storage. *Adv. Funct. Mater.* **2017**, *27* (29), 1700447.

(13) Yang, C.; Fu, K.; Zhang, Y.; Hitz, E.; Hu, L. Protected Lithium-Metal Anodes in Batteries: From Liquid to Solid. *Adv. Mater.* **2017**, *29* (36), 1701169.

(14) Liu, B.; Zhang, L.; Xu, S.; McOwen, D. W.; Gong, Y.; Yang, C.; Pastel, G. R.; Xie, H.; Fu, K.; Dai, J.; Chen, C.; Wachsman, E. D.; Hu, L. 3D Lithium Metal Anodes Hosted in Asymmetric Garnet Frameworks toward High Energy Density Batteries. *Energy Storage Mater.* **2018**, *14*, 376−382.

(15) Wang, H.; Yu, D.; Kuang, C.; Cheng, L.; Li, W.; Feng, X.; Zhang, Z.; Zhang, X.; Zhang, Y. Alkali Metal Anodes for Rechargeable Batteries. *Chem.* **2019**, *5* (2), 313−338.

(16) Guo, Y.; Li, H.; Zhai, T. Reviving Lithium-Metal Anodes for Next-Generation High-Energy Batteries. *Adv. Mater.* **2017**, *29* (29), 1700007.

(17) Lewis, J. A.; Cortes, F. J. Q.; Boebinger, M. G.; Tippens, J.; Marchese, T. S.; Kondekar, N.; Liu, X.; Chi, M.; McDowell, M. T. Interphase Morphology between a Solid-State Electrolyte and Lithium Controls Cell Failure. *ACS Energy Lett.* **2019**, *4* (2), 591−599.

(18) Zhang, W.; Schröder, D.; Arlt, T.; Manke, I.; Koerver, R.; Pinedo, R.; Weber, D. A.; Sann, J.; Zeier, W. G.; Janek, J. (Electro)Chemical Expansion during Cycling: Monitoring the Pressure Changes in Operating Solid-State Lithium Batteries. *J. Mater. Chem. A* **2017**, *5* (20), 9929−9936.

(19) Porz, L.; Swamy, T.; Sheldon, B. W.; Rettenwander, D.; Frömling, T.; Thaman, H. L.; Berendts, S.; Uecker, R.; Carter, W. C.; Chiang, Y. M. Mechanism of Lithium Metal Penetration through Inorganic Solid Electrolytes. *Adv. Energy Mater.* **2017**, *7* (20), 1701003.

(20) Nam, Y. J.; Park, K. H.; Oh, D. Y.; An, W. H.; Jung, Y. S. Diagnosis of Failure Modes for All-Solid-State Li-Ion Batteries Enabled by Three-Electrode Cells. *J. Mater. Chem. A* **2018**, *6* (30), 14867−14875.

(21) Song, Y.; Yang, L.; Zhao, W.; Wang, Z.; Zhao, Y.; Wang, Z.; Zhao, Q.; Liu, H.; Pan, F. Revealing the Short-Circuiting Mechanism of Garnet-Based Solid-State Electrolyte. *Adv. Energy Mater.* **2019**, *9* (21), 1900671.

(22) Pervez, S. A.; Cambaz, M. A.; Thangadurai, V.; Fichtner, M. Interface in Solid-State Lithium Battery: Challenges, Progress, and Outlook. *ACS Appl. Mater. Interfaces* **2019**, *11*, 22029−22050.

(23) Xiao, Y.; Wang, Y.; Bo, S. H.; Kim, J. C.; Miara, L. J.; Ceder, G. Understanding Interface Stability in Solid-State Batteries. *Nat. Rev. Mater.* **2020**, *5* (2), 105−126.

(24) Riphaus, N.; Stiaszny, B.; Beyer, H.; Indris, S.; Gasteiger, H. A.; Sedlmaier, S. J. Editors' Choice—Understanding Chemical Stability Issues between Different Solid Electrolytes in All-Solid-State Batteries. *J. Electrochem. Soc.* **2019**, *166* (6), A975−A983.

(25) Duan, J.; Wu, W.; Nolan, A. M.; Wang, T.; Wen, J.; Hu, C.; Mo, Y.; Luo, W.; Huang, Y. Lithium−Graphite Paste: An Interface Compatible Anode for Solid-State Batteries. *Adv. Mater.* **2019**, *31* (10), 1807243.

(26) Wenzel, S.; Sedlmaier, S. J.; Dietrich, C.; Zeier, W. G.; Janek, J. Interfacial Reactivity and Interphase Growth of Argyrodite Solid Electrolytes at Lithium Metal Electrodes. *Solid State Ionics* **2018**, *318*, 102−112.

(27) Fan, L.; Wei, S.; Li, S.; Li, Q.; Lu, Y. Recent Progress of the Solid-State Electrolytes for High-Energy Metal-Based Batteries. *Adv. Energy Mater.* **2018**, *8* (11), 1702657.

(28) Tantratian, K.; Cao, D.; Abdelaziz, A.; Sun, X.; Sheng, J.; Natan, A.; Chen, L.; Zhu, H. Stable Li Metal Anode Enabled by Space Confinement and Uniform Curvature through Lithiophilic Nanotube Arrays. *Adv. Energy Mater.* **2020**, *10* (5), 1902819.

(29) Cengiz, M.; Oh, H.; Lee, S.-H. Lithium Dendrite Growth Suppression and Ionic Conductivity of Li 2 S-P 2 S 5 -P 2 O 5 Glass Solid Electrolytes Prepared by Mechanical Milling. *J. Electrochem. Soc.* **2019**, *166* (16), A3997−A4004.

(30) Cao, D.; Sun, X.; Li, Q.; Natan, A.; Xiang, P.; Zhu, H. Lithium Dendrite in All-Solid-State Batteries: Growth Mechanisms, Suppression Strategies, and Characterizations. *Matter* **2020**, *3* (1), 57−94.

(31) Chen, Y.; Wang, Z.; Li, X.; Yao, X.; Wang, C.; Li, Y.; Xue, W.; Yu, D.; Kim, S. Y.; Yang, F.; Kushima, A.; Zhang, G.; Huang, H.; Wu, N.; Mai, Y. W.; Goodenough, J. B.; Li, J. Li Metal Deposition and Stripping in a Solid-State Battery via Coble Creep. *Nature* **2020**, *578* (7794), 251−255.

(32) Li, X.; Jin, L.; Song, D.; Zhang, H.; Shi, X.; Wang, Z.; Zhang, L.; Zhu, L. LiNbO3-Coated LiNi0.8Co0.1Mn0.1O2 Cathode with High Discharge Capacity and Rate Performance for All-Solid-State Lithium Battery. *J. Energy Chem.* **2020**, *40*, 39−45.

https://doi.org/10.1021/acsenergylett.1c00627
ACS Energy Lett. 2021, 6, 1831−1838

(33) Yersak, T.; Salvador, J. R.; Schmidt, R. D.; Cai, M. Hot Pressed, Fiber-Reinforced (Li2S)70(P2S5)30 Solid-State Electrolyte Separators for Li Metal Batteries. *ACS Appl. Energy Mater.* **2019**, *2* (5), 3523−3531.
(34) Ye, H.; Xin, S.; Yin, Y. X.; Li, J. Y.; Guo, Y. G.; Wan, L. J. Stable Li Plating/Stripping Electrochemistry Realized by a Hybrid Li Reservoir in Spherical Carbon Granules with 3D Conducting Skeletons. *J. Am. Chem. Soc.* **2017**, *139* (16), 5916−5922.
(35) Yoshinari, T.; Koerver, R.; Hofmann, P.; Uchimoto, Y.; Zeier, W. G.; Janek, J. Interfacial Stability of Phosphate-NASICON Solid Electrolytes in Ni-Rich NCM Cathode-Based Solid-State Batteries. *ACS Appl. Mater. Interfaces* **2019**, *11* (26), 23244−23253.
(36) Chi, S.-S.; Liu, Y.; Zhao, N.; Guo, X.; Nan, C. W.; Fan, L. Z. Solid Polymer Electrolyte Soft Interface Layer with 3D Lithium Anode for All-Solid-State Lithium Batteries. *Energy Storage Mater.* **2019**, *17*, 309−316.
(37) Lim, H. D.; Lim, H. K.; Xing, X.; Lee, B. S.; Liu, H.; Coaty, C.; Kim, H.; Liu, P. Solid Electrolyte Layers by Solution Deposition. *Adv. Mater. Interfaces* **2018**, *5* (8), 1701328.
(38) Han, F.; Westover, A. S.; Yue, J.; Fan, X.; Wang, F.; Chi, M.; Leonard, D. N.; Dudney, N. J.; Wang, H.; Wang, C. High Electronic Conductivity as the Origin of Lithium Dendrite Formation within Solid Electrolytes. *Nat. Energy* **2019**, *4* (3), 187−196.
(39) Lim, H. D.; Yue, X.; Xing, X.; Petrova, V.; Gonzalez, M.; Liu, H.; Liu, P. Designing Solution Chemistries for the Low-Temperature Synthesis of Sulfide-Based Solid Electrolytes. *J. Mater. Chem. A* **2018**, *6* (17), 7370−7374.
(40) Xu, S.; McOwen, D. W.; Wang, C.; Zhang, L.; Luo, W.; Chen, C.; Li, Y.; Gong, Y.; Dai, J.; Kuang, Y.; Yang, C.; Hamann, T. R.; Wachsman, E. D.; Hu, L. Three-Dimensional, Solid-State Mixed Electron-Ion Conductive Framework for Lithium Metal Anode. *Nano Lett.* **2018**, *18* (6), 3926−3933.
(41) Yin, L.; Wang, J.; Lin, F.; Yang, J.; Nuli, Y. Polyacrylonitrile/Graphene Composite as a Precursor to a Sulfur-Based Cathode Material for High-Rate Rechargeable Li-S Batteries. *Energy Environ. Sci.* **2012**, *5* (5), 6966−6972.
(42) Wood, K. N.; Steirer, K. X.; Hafner, S. E.; Ban, C.; Santhanagopalan, S.; Lee, S. H.; Teeter, G. Operando X-Ray Photoelectron Spectroscopy of Solid Electrolyte Interphase Formation and Evolution in Li2S-P2S5 Solid-State Electrolytes. *Nat. Commun.* **2018**, *9* (1), 1−10.
(43) Liu, H.; Yue, X.; Xing, X.; Yan, Q.; Huang, J.; Petrova, V.; Zhou, H.; Liu, P. A Scalable 3D Lithium Metal Anode. *Energy Storage Mater.* **2019**, *16*, 505−511.
(44) Zhang, Y.; Liu, B.; Hitz, E.; Luo, W.; Yao, Y.; Li, Y.; Dai, J.; Chen, C.; Wang, Y.; Yang, C.; Li, H.; Hu, L. A Carbon-Based 3D Current Collector with Surface Protection for Li Metal Anode. *Nano Res.* **2017**, *10* (4), 1356−1365.
(45) Zhang, Q.; Cao, D.; Ma, Y.; Natan, A.; Aurora, P.; Zhu, H. Sulfide-Based Solid-State Electrolytes: Synthesis, Stability, and Potential for All-Solid-State Batteries. *Adv. Mater.* **2019**, *31* (44), 1901131.
(46) Park, K. H.; Bai, Q.; Kim, D. H.; Oh, D. Y.; Zhu, Y.; Mo, Y.; Jung, Y. S. Design Strategies, Practical Considerations, and New Solution Processes of Sulfide Solid Electrolytes for All-Solid-State Batteries. *Adv. Energy Mater.* **2018**, *8* (18), 1800035.
(47) Duan, J.; Zheng, Y.; Luo, W.; Wu, W.; Wang, T.; Xie, Y.; Li, S.; Li, J.; Huang, Y. Is Graphite Lithiophobic or Lithiophilic? *Natl. Sci. Rev.* **2020**, *7* (7), 1208−1217.
(48) Liang, Z.; Lin, D.; Zhao, J.; Lu, Z.; Liu, Y.; Liu, C.; Lu, Y.; Wang, H.; Yan, K.; Tao, X.; Cui, Y. Composite Lithium Metal Anode by Melt Infusion of Lithium into a 3D Conducting Scaffold with Lithiophilic Coating. *Proc. Natl. Acad. Sci. U. S. A.* **2016**, *113* (11), 2862−2867.
(49) Lim, H. D.; Yue, X.; Xing, X.; Petrova, V.; Gonzalez, M.; Liu, H.; Liu, P. Designing Solution Chemistries for the Low-Temperature Synthesis of Sulfide-Based Solid Electrolytes. *J. Mater. Chem. A* **2018**, *6* (17), 7370−7374.
(50) Kudu, Ö. U.; Famprikis, T.; Fleutot, B.; Braida, M. D.; Le Mercier, T.; Islam, M. S.; Masquelier, C. A Review of Structural Properties and Synthesis Methods of Solid Electrolyte Materials in the Li2S − P2S5 Binary System. *J. Power Sources* **2018**, *407*, 31−43.
(51) Sun, Y.; Zheng, G.; Seh, Z. W.; Liu, N.; Wang, S.; Sun, J.; Lee, H. R.; Cui, Y. Graphite-Encapsulated Li-Metal Hybrid Anodes for High-Capacity Li Batteries. *Chem.* **2016**, *1* (2), 287−297.
(52) Zhao, Q.; Hao, X.; Su, S.; Ma, J.; Hu, Y.; Liu, Y.; Kang, F.; He, Y. B. Expanded-Graphite Embedded in Lithium Metal as Dendrite-Free Anode of Lithium Metal Batteries. *J. Mater. Chem. A* **2019**, *7* (26), 15871−15879.
(53) Shi, P.; Li, T.; Zhang, R.; Shen, X.; Cheng, X. B.; Xu, R.; Huang, J. Q.; Chen, X. R.; Liu, H.; Zhang, Q. Lithiophilic LiC 6 Layers on Carbon Hosts Enabling Stable Li Metal Anode in Working Batteries. *Adv. Mater.* **2019**, *31* (8), 1807131.
(54) Chen, S.; Xie, D.; Liu, G.; Mwizerwa, J. P.; Zhang, Q.; Zhao, Y.; Xu, X.; Yao, X. Sulfide Solid Electrolytes for All-Solid-State Lithium Batteries: Structure, Conductivity, Stability and Application. *Energy Storage Mater.* **2018**, *14*, 58−74.
(55) Dash, R.; Pannala, S. Theoretical Limits of Energy Density in Silicon-Carbon Composite Anode Based Lithium Ion Batteries. *Sci. Rep.* **2016**, *6* (June), 6−12.
(56) Schnell, J.; Günther, T.; Knoche, T.; Vieider, C.; Köhler, L.; Just, A.; Keller, M.; Passerini, S.; Reinhart, G. All-Solid-State Lithium-Ion and Lithium Metal Batteries − Paving the Way to Large-Scale Production. *J. Power Sources* **2018**, *382*, 160−175.
(57) Han, F.; Yue, J.; Zhu, X.; Wang, C. Suppressing Li Dendrite Formation in Li2S-P2S5 Solid Electrolyte by LiI Incorporation. *Adv. Energy Mater.* **2018**, *8* (18), 1703644.
(58) Zhang, N.; Long, X.; Wang, Z.; Yu, P.; Han, F.; Fu, J.; Ren, G.; Wu, Y.; Zheng, S.; Huang, W.; Wang, C.; Li, H.; Liu, X. Mechanism Study on the Interfacial Stability of a Lithium Garnet-Type Oxide Electrolyte against Cathode Materials. *ACS Appl. Energy Mater.* **2018**, *1* (11), 5968−5976.
(59) Liu, H.; Zhu, Z.; Huang, J.; He, X.; Chen, Y.; Zhang, R.; Lin, R.; Li, Y.; Yu, S.; Xing, X.; Yan, Q.; Li, X.; Frost, M. J.; An, K.; Feng, J.; Kostecki, R.; Xin, H.; Ong, S. P.; Liu, P. Elucidating the Limit of Li Insertion into the Spinel Li4Ti5O12. *ACS Mater. Lett.* **2019**, *1* (1), 96−102.
(60) Xu, L.; Tang, S.; Cheng, Y.; Wang, K.; Liang, J.; Liu, C.; Cao, Y. C.; Wei, F.; Mai, L. Interfaces in Solid-State Lithium Batteries. *Joule* **2018**, *2* (10), 1991−2015.
(61) Xin, F.; Zhou, H.; Chen, X.; Zuba, M.; Chernova, N.; Zhou, G.; Whittingham, M. S. Li-Nb-O Coating/Substitution Enhances the Electrochemical Performance of the LiNi0.8Mn0.1Co0.1O2 (NMC 811) Cathode. *ACS Appl. Mater. Interfaces* **2019**, *11* (38), 34889−34894.
(62) Özer, N.; Lampert, C. M. Electrochemical Lithium Insertion in Sol-Gel Deposited LiNbO3 Films. *Sol. Energy Mater. Sol. Cells* **1995**, *39* (2−4), 367−375.
(63) Yanovskaya, M. I.; Turevskaya, E. P.; Leonov, A. P.; Ivanov, S. A.; Kolganova, N. V.; Stefanovich, S. Y.; Turova, N. Y.; Venevtsev, Y. N. Formation of LiNbO3 Powders and Thin Films by Hydrolysis of Metal Alkoxides. *J. Mater. Sci.* **1988**, *23* (2), 395−399.
(64) Judez, X.; Eshetu, G. G.; Li, C.; Rodriguez-Martinez, L. M.; Zhang, H.; Armand, M. Opportunities for Rechargeable Solid-State Batteries Based on Li-Intercalation Cathodes. *Joule* **2018**, *2* (11), 2208−2224.
(65) Wu, F.; Yushin, G. Conversion Cathodes for Rechargeable Lithium and Lithium-Ion Batteries. *Energy Environ. Sci.* **2017**, *10* (2), 435−459.
(66) Du, M.; Liao, K.; Lu, Q.; Shao, Z. Recent Advances in the Interface Engineering of Solid-State Li-Ion Batteries with Artificial Buffer Layers: Challenges, Materials, Construction, and Characterization. *Energy Environ. Sci.* **2019**, *12* (6), 1780−1804.

https://doi.org/10.1021/acsenergylett.1c00627
ACS Energy Lett. 2021, 6, 1831−1838